Inorganic Chemistry
Article

Inorg. Chem. **2010**, *49*, 10133–10143 **10133**
DOI: 10.1021/ic101517t

Two-Step Adsorption on Jungle-Gym-Type Porous Coordination Polymers: Dependence on Hydrogen-Bonding Capability of Adsorbates, Ligand-Substituent Effect, and Temperature

Kazuhiro Uemura,*,† Yukari Yamasaki,‡ Fumiaki Onishi,‡ Hidetoshi Kita,‡ and Masahiro Ebihara†

†*Department of Chemistry, Faculty of Engineering, Gifu University, Yanagido 1-1, Gifu, 501-1193, Japan, and* ‡*Environmental Science and Engineering, Graduate School of Science and Engineering, Yamaguchi University, Tokiwadai 2-16-1, Ube-shi, Yamaguchi 755-8611, Japan*

Received July 28, 2010

A preliminary study of isopropanol (IPA) adsorption/desorption isotherms on a jungle-gym-type porous coordination polymer, $[Zn_2(bdc)_2(dabco)]_n$ (**1**, H_2bdc = 1,4-benzenedicarboxylic acid, dabco =1,4-diazabicyclo[2.2.2]octane), showed unambiguous two-step profiles via a highly shrunk intermediate framework. The results of adsorption measurements on **1**, using probing gas molecules of alcohol (MeOH and EtOH) for the size effect and Me_2CO for the influence of hydrogen bonding, show that alcohol adsorption isotherms are gradual two-step profiles, whereas the Me_2CO isotherm is a typical type-I isotherm, indicating that a two-step adsorption/desorption is involved with hydrogen bonds. To further clarify these characteristic adsorption/desorption behaviors, selecting nitroterephthalate (bdc-NO_2), bromoterephthalate (bdc-Br), and 2,5-dichloroterephthalate (bdc-Cl_2) as substituted dicarboxylate ligands, isomorphous jungle-gym-type porous coordination polymers, $\{[Zn_2(bdc\text{-}NO_2)_2(dabco)]\cdot solvents\}_n$ (**2** ⊃ *solvents*), $\{[Zn_2(bdc\text{-}Br)_2(dabco)]\cdot solvents\}_n$ (**3** ⊃ *solvents*), and $\{[Zn_2(bdc\text{-}Cl_2)_2(dabco)]\cdot solvents\}_n$ (**4** ⊃ *solvents*), were synthesized and characterized by single-crystal X-ray analyses. Thermal gravimetry, X-ray powder diffraction, and N_2 adsorption at 77 K measurements reveal that $[Zn_2(bdc\text{-}NO_2)_2(dabco)]_n$ (**2**), $[Zn_2(bdc\text{-}Br)_2(dabco)]_n$ (**3**), and $[Zn_2(bdc\text{-}Cl_2)_2(dabco)]_n$ (**4**) maintain their frameworks without guest molecules with Brunauer−Emmett−Teller (BET) surface areas of 1568 (**2**), 1292 (**3**), and 1216 (**4**) $m^2\ g^{-1}$. As found in results of MeOH, EtOH, IPA, and Me_2CO adsorption/desorption on **2**−**4**, only MeOH adsorption on **2** shows an obvious two-step profile. Considering the substituent effects and adsorbate sizes, the hydrogen bonds, which are triggers for two-step adsorption, are formed between adsorbates and carboxylate groups at the corners in the pores, inducing wide pores to become narrow pores. Interestingly, such a two-step MeOH adsorption on **2** depends on the temperature, attributed to the small free-energy difference (ΔF_{host}) between the two guest-free forms, wide and narrow pores.

Introduction

Porous coordination polymers with structurally well-defined nanoscale cavities are of great interest[1] because of their unique properties, such as gas storage,[2] separation,[3] and catalysis,[4] which are all associated with the presence of functional pores. Numerous types of porous coordination polymers, namely, open metal−organic frameworks, have been synthesized and constructed with judicious choices of metals and designed bridging ligands affording tailored open channels and cavities.[1,5,6]

*To whom correspondence should be addressed. E-mail: k_uemura@gifu-u.ac.jp. Phone: 81-58-293-2561. Fax: 81-58-293-2794.

(1) (a) Yaghi, O. M.; O'Keeffe, M.; Ockwig, N. W.; Chae, H. K.; Eddaoudi, M.; Kim, J. *Nature* **2003**, *423*, 705–714. (b) James, S. L. *Chem. Soc. Rev.* **2003**, *32*, 276–288. (c) Janiak, C. *Dalton Trans.* **2003**, 2781–2804. (d) Kitagawa, S.; Kitaura, R.; Noro, S.-i. *Angew. Chem., Int. Ed.* **2004**, *43*, 2334–2375. (e) Férey, G.; Mellot-Draznieks, C.; Serre, C.; Millange, F. *Acc. Chem. Res.* **2005**, *38*, 217–225.

(2) (a) Morris, R. E.; Wheatley, P. S. *Angew. Chem., Int. Ed.* **2008**, *47*, 4966–4981. (b) Dincă, M.; Long, J. R. *Angew. Chem., Int. Ed.* **2008**, *47*, 6766–6779. (c) Murray, L. J.; Dincă, M.; Long, J. R. *Chem. Soc. Rev.* **2009**, *38*, 1294–1314. (d) Thomas, K. M. *Dalton Trans.* **2009**, 1487–1505.

(3) Li, J.-R.; Kuppler, R. J.; Zhou, H.-C. *Chem. Soc. Rev.* **2009**, *38*, 1477–1504.

(4) (a) Ma, L.; Abney, C.; Lin, W. *Chem. Soc. Rev.* **2009**, *38*, 1248–1256. (b) Lee, J.; Farha, O. K.; Roberts, J.; Scheidt, K. A.; Nguyen, S. T.; Hupp, J. T. *Chem. Soc. Rev.* **2009**, *38*, 1450–1459. (c) Farrusseng, D.; Aguado, S.; Pinel, C. *Angew. Chem., Int. Ed.* **2009**, *48*, 7502–7513.

(5) (a) Dybtsev, D. N.; Chun, H.; Kim, K. *Angew. Chem., Int. Ed.* **2004**, *43*, 5033–5036. (b) Chun, H.; Dybtsev, D. N.; Kim, H.; Kim, K. *Chem. Eur. J.* **2005**, *11*, 3521–3529.

(6) Recent jungle-gym-type porous coordination polymers: (a) Seki, K.; Takamizawa, S.; Mori, W. *Chem. Lett.* **2001**, 332–333. (b) Seki, K.; Mori, W. *J. Phys. Chem. B* **2002**, *106*, 1380–1385. (c) Kitaura, R.; Iwahori, F.; Matsuda, R.; Kitagawa, S.; Kubota, Y.; Takata, M.; Kobayashi, T. C. *Inorg. Chem.* **2004**, *43*, 6522–6524. (d) Mori, W.; Sato, T.; Ohmura, T.; Kato, C. N.; Takei, T. *J. Solid State Chem.* **2005**, *178*, 2555–2573. (e) Ma, B.-Q.; Mulfort, K. L.; Hupp, J. T. *Inorg. Chem.* **2005**, *44*, 4912–4914. (f) Chen, B.; Liang, C.; Yang, J.; Contreras, D. S.; Clancy, Y. L.; Lobkovsky, E. B.; Yaghi, O. M.; Dai, S. *Angew. Chem., Int. Ed.* **2006**, *45*, 1390–1393. (g) Chen, B.; Ma, S.; Zapata, F.; Lobkovsky, E. B.; Yang, J. *Inorg. Chem.* **2006**, *45*, 5718–5720. (h) Tanaka, D.; Horike, S.; Kitagawa, S.; Ohba, M.; Hasegawa, M.; Ozawa, Y.; Toriumi, K. *Chem. Commun.* **2007**, 3142–3144. (i) Chen, B.; Ma, S.; Zapata, F.; Fronczek, F. R.; Lobkovsky, E. B.; Zhou, H.-C. *Inorg. Chem.* **2007**, *46*, 1233–1236. (j) Dybtsev, D. N.; Yutkin, M. P.; Peresypkina, E. V.; Virovets, A. V.; Serre, C.; Férey, G.; Fedin, V. P. *Inorg. Chem.* **2007**, *46*, 6843–6845. (k) Tanaka, D.; Higuchi, M.; Horike, S.; Matsuda, R.; Kinoshita, Y.; Yanai, N.; Kitagawa, S. *Chem. Asian J.* **2008**, *3*, 1343–1349. (l) Li, K.; Lee, J. Y.; Olson, D. H.; Emge, T. J.; Bi, W.; Eibling, M. J.; Li, J. *Chem. Commun.* **2008**, 6123–6125. (m) Wang, Z.; Tanabe, K. K.; Cohen, S. M. *Inorg. Chem.* **2009**, *48*, 296–306.

Published on Web 10/07/2010

The interesting aspect found in those open spaces is their framework's flexibilities,[7,8] where pore shapes and sizes change in response to penetrating guest molecules with maintaining of the framework in the solid state. Such a stimulus-driven structural responsiveness is rarely observed in other classes of porous materials such as zeolites and activated carbons, and therefore provides a unique entry into the development of functional materials for gas separation and sensing.[8]

The framework flexibilities reflect characteristic adsorption isotherm profiles, which are impossible to be grouped into the IUPAC classification[9] for adsorption isotherms. Those characteristic isotherm profiles are roughly divided into two types. One is an isotherm containing a threshold pressure,[10] defined as the "gate pressure",[10a] where adsorption amounts suddenly increase at that pressure, as shown in Scheme 1a. The other type is a stepwise isotherm,[6f,k,l,11−13] whose behavior in porous coordination polymers is best exemplified by MIL-53,[12] where a wide → narrow → wide pore transition with gas filling has been observed (Scheme 1b), termed the "breathing effect".[8] Both types of isotherms show obvious hysteresis loops. From a thermodynamic point of view, gate pressure was recognized as the equilibrium pressure between the initial (closed form) and final (open form) states;[10e,h] however, the adsorption

Scheme 1

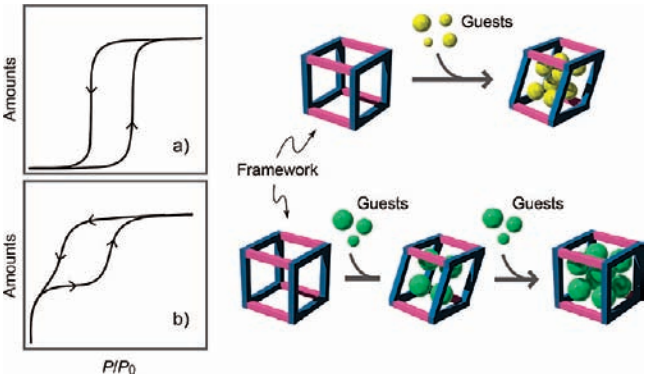

mechanisms that have been reported to date for the stepwise isotherms except for MIL-53[12] are still difficult to understand.

It has been pointed out that the breathing effect produced by distortion around the secondary building unit (SBU) is allowed only for SBUs possessing a crystallographic mirror plane.[8] For example, a family of highly porous IRMOFs, which have a cubic structure, constructed using $Zn_4O(CO_2)_6$ as the SBU,[14] is inhibited from demonstrating the breathing effect because of the absence of a mirror plane in $Zn_4O(CO_2)_6$.[8] In contrast, in MIL-53, the planes consisting of metals and a coordinated carboxylate group are perpendicular to each other (Scheme 2), which allows a hinge-like motion around the metals, producing framework flexibility.[12] Similarly to MIL-53, the paddle-wheel unit, $Zn_2(CO_2)_4(L)$ (L = nitrogen donor ligand),[5,6,13] which is another SBU with a different connectivity from $Zn_4O(CO_2)_6$, typically resulting in a tetragonal (distorted cubic) structure, is allowed to breathe. Actually, $[Zn_2(bdc)_2(dabco)]_n$ (**1**, H_2bdc = 1,4-benzenedicarboxylic acid, dabco = 1,4-diazabicyclo[2.2.2]octane)[5] shows an unambiguous two-step process for isopropanol (IPA)

(7) (a) Kitagawa, S.; Uemura, K. *Chem. Soc. Rev.* **2005**, *34*, 109–119. (b) Uemura, K.; Matsuda, R.; Kitagawa, S. *J. Solid State Chem.* **2005**, *178*, 2420–2429. (c) Fletcher, A. J.; Thomas, K. M.; Rosseinsky, M. J. *J. Solid State Chem.* **2005**, *178*, 2491–2510. (d) Horike, S.; Shimomura, S.; Kitagawa, S. *Nat. Chem.* **2009**, *1*, 695–704.

(8) Férey, G.; Serre, C. *Chem. Soc. Rev.* **2009**, *38*, 1380–1399.

(9) Rouquerol, F.; Rouquerol, J.; Sing, K. *Adsorption by Powders and Porous Solids*; Academic Press: London, 1999.

(10) For examples of "gate pressures": (a) Li, D.; Kaneko, K. *Chem. Phys. Lett.* **2001**, *335*, 50–56. (b) Kitaura, R.; Fujimoto, K.; Noro, S.-i.; Kondo, M.; Kitagawa, S. *Angew. Chem., Int. Ed.* **2002**, *41*, 133–135. (c) Seki, K. *Phys. Chem. Chem. Phys.* **2002**, *4*, 1968–1971. (d) Uemura, K.; Kitagawa, S.; Kondo, M.; Fukui, K.; Kitaura, R.; Chang, H.-C.; Mizutani, T. *Chem. Eur. J.* **2002**, *8*, 3586–3600. (e) Uemura, K.; Kitagawa, S.; Fukui, K.; Saito, K. *J. Am. Chem. Soc.* **2004**, *126*, 3817–3828. (f) Maji, T. K.; Mostafa, G.; Matsuda, R.; Kitagawa, S. *J. Am. Chem. Soc.* **2005**, *127*, 17152–17153. (g) Noguchi, H.; Kondoh, A.; Hattori, Y.; Kanoh, H.; Kajiro, H.; Kaneko, K. *J. Phys. Chem. B* **2005**, *109*, 13851–13853. (h) Uemura, K.; Kitagawa, S.; Saito, K.; Fukui, K.; Matsumoto, K. *J. Therm. Anal. Calorim.* **2005**, *81*, 529–532. (i) Kondo, A.; Noguchi, H.; Ohnishi, S.; Kajiro, H.; Tohdoh, A.; Hattori, Y.; Xu, W.-C.; Tanaka, H.; Kanoh, H.; Kaneko, K. *Nano Lett.* **2006**, *6*, 2581–2584. (j) Takamizawa, S.; Kojima, K.; Akatsuka, T. *Inorg. Chem.* **2006**, *45*, 4580–4582. (k) Shimomura, S.; Horike, S.; Matsuda, R.; Kitagawa, S. *J. Am. Chem. Soc.* **2007**, *129*, 10990–10991. (l) Noguchi, H.; Kondo, A.; Hattori, Y.; Kajiro, H.; Kanoh, H.; Kaneko, K. *J. Phys. Chem. C* **2007**, *111*, 248–254. (m) Tanaka, D.; Nakagawa, K.; Higuchi, M.; Horike, S.; Kubota, Y.; Kobayashi, T. C.; Takata, M.; Kitagawa, S. *Angew. Chem., Int. Ed.* **2008**, *47*, 3914–3918. (n) Choi, H.-S.; Suh, M. P. *Angew. Chem., Int. Ed.* **2009**, *48*, 6865–6869. (o) Ghosh, S. K.; Azhakar, R.; Kitagawa, S. *Chem. Asian J.* **2009**, *4*, 870–875.

(11) For examples of stepwise adsorption behaviors: (a) Fletcher, A. J.; Cussen, E. J.; Prior, T. J.; Rosseinsky, M. J.; Kepert, C. J.; Thomas, K. M. *J. Am. Chem. Soc.* **2001**, *123*, 10001–10011. (b) Takamizawa, S.; Saito, T.; Akatsuka, T.; Nakata, E.-i. *Inorg. Chem.* **2005**, *44*, 1421–1424. (c) Yamada, K.; Tanaka, H.; Yagishita, S.; Adachi, K.; Uemura, T.; Kitagawa, S.; Kawata, S. *Inorg. Chem.* **2006**, *45*, 4322–4324. (d) Kondo, A.; Noguchi, H.; Carlucci, L.; Proserpio, D. M.; Ciani, G.; Kajiro, H.; Ohba, T.; Kanoh, H.; Kaneko, K. *J. Am. Chem. Soc.* **2007**, *129*, 12362–12363. (e) Zhang, J.-P.; Kitagawa, S. *J. Am. Chem. Soc.* **2008**, *130*, 907–917. (f) Culp, J. T.; Smith, M. R.; Bittner, E.; Bockrath, B. *J. Am. Chem. Soc.* **2008**, *130*, 12427–12434. (g) Higuchi, M.; Tanaka, D.; Horike, S.; Sakamoto, H.; Nakamura, K.; Takashima, Y.; Hijikata, Y.; Yanai, N.; Kim, J.; Kato, K.; Kubota, Y.; Takata, M.; Kitagawa, S. *J. Am. Chem. Soc.* **2009**, *131*, 10336–10337. (h) Seo, J.; Matsuda, R.; Sakamoto, H.; Bonneau, C.; Kitagawa, S. *J. Am. Chem. Soc.* **2009**, *131*, 12792–12800. (i) Takamizawa, S.; Takasaki, Y.; Miyake, R. *Chem. Commun.* **2009**, 6625–6627. (j) Noro, S.-i.; Tanaka, D.; Sakamoto, H.; Shimomura, S.; Kitagawa, S.; Takeda, S.; Uemura, K.; Kita, H.; Akutagawa, T.; Nakamura, T. *Chem. Mater.* **2009**, *21*, 3346–3355. (k) Zhang, J.-P.; Ghosh, S. K.; Lin, J.-B.; Kitagawa, S. *Inorg. Chem.* **2009**, *48*, 7970–7976. (l) Park, H. J.; Suh, M. P. *Chem. Commun.* **2010**, *46*, 610–612. (m) Mulfort, K. L.; Farha, O. K.; Malliakas, C. D.; Kanatzidis, M. G.; Hupp, J. T. *Chem. Eur. J.* **2010**, *16*, 276–281.

(12) Selected stepwise adsorption behaviors on MIL-53: (a) Bourrelly, S.; Llewellyn, P. L.; Serre, C.; Millange, F.; Loiseau, T.; Férey, G. *J. Am. Chem. Soc.* **2005**, *127*, 13519–13521. (b) Llewellyn, P. L.; Bourrelly, S.; Serre, C.; Filinchuk, Y.; Férey, G. *Angew. Chem., Int. Ed.* **2006**, *45*, 7751–7754. (c) Serre, C.; Bourrelly, S.; Vimont, A.; Ramsahye, N. A.; Maurin, G.; Llewellyn, P. L.; Daturi, M.; Filinchuk, Y.; Leynaud, O.; Barnes, P.; Férey, G. *Adv. Mater.* **2007**, *19*, 2246–2251. (d) Liu, Y.; Her, J.-H.; Dailly, A.; Ramirez-Cuesta, A. J.; Neumann, D. A.; Brown, C. M. *J. Am. Chem. Soc.* **2008**, *130*, 11813–11818. (e) Llewellyn, P. L.; Maurin, G.; Devic, T.; Loera-Serna, S.; Rosenbach, N.; Serre, C.; Bourrelly, S.; Horcajada, P.; Filinchuk, Y.; Férey, G. *J. Am. Chem. Soc.* **2008**, *130*, 12808–12814. (f) Trung, T. K.; Trens, P.; Tanchoux, N.; Bourrelly, S.; Llewellyn, P. L.; Loera-Serna, S.; Serre, C.; Loiseau, T.; Fajula, F.; Férey, G. *J. Am. Chem. Soc.* **2008**, *130*, 16926–16932. (g) Ramsahye, N. A.; Maurin, G.; Bourrelly, S.; Llewellyn, P. L.; Serre, C.; Loiseau, T.; Devic, T.; Férey, G. *J. Phys. Chem. C* **2008**, *112*, 514–520. (h) Hamon, L.; Serre, C.; Devic, T.; Loiseau, T.; Millange, F.; Férey, G.; Weireld, G. D. *J. Am. Chem. Soc.* **2009**, *131*, 8775–8777. (i) Llewellyn, P. L.; Horcajada, P.; Maurin, G.; Devic, T.; Rosenbach, N.; Bourrelly, S.; Serre, C.; Vincent, D.; Loera-Serna, S.; Filinchuk, Y.; Férey, G. *J. Am. Chem. Soc.* **2009**, *131*, 13002–13008. (j) Devic, T.; Horcajada, P.; Serre, C.; Salles, F.; Maurin, G.; Moulin, B.; Heurtaux, D.; Clet, G.; Vimont, A.; Grenèche, J.-M.; Ouay, B. L.; Moreau, F.; Magnier, E.; Filinchuk, Y.; Marrot, J.; Lavalley, J.-C.; Daturi, M.; Férey, G. *J. Am. Chem. Soc.* **2010**, *132*, 1127–1136. (k) Bourrelly, S.; Moulin, B.; Rivera, A.; Maurin, G.; Devautour-Vinot, S.; Serre, C.; Devic, T.; Horcajada, P.; Vimont, A.; Clet, G.; Daturi, M.; Lavalley, J.-C.; Loera-Serna, S.; Denoyel, R.; Llewellyn, P. L.; Férey, G. *J. Am. Chem. Soc.* **2010**, *132*, 9488–9498.

(13) (a) Uemura, K.; Yamasaki, Y.; Komagawa, Y.; Tanaka, K.; Kita, H. *Angew. Chem., Int. Ed.* **2007**, *46*, 6662–6665. (b) Uemura, K.; Komagawa, Y.; Yamasaki, Y.; Kita, H. *Desalination* **2008**, *234*, 1–8. (c) Uemura, K.; Onishi, F.; Yamasaki, Y.; Kita, H. *J. Solid State Chem.* **2009**, *182*, 2852–2857.

(14) (a) Li, H.; Eddaoudi, M.; O'Keeffe, M.; Yaghi, O. M. *Nature* **1999**, *402*, 276–279. (b) Eddaoudi, M.; Kim, J.; Rosi, N.; Vodak, D.; Wachter, J.; O'Keeffe, M.; Yaghi, O. M. *Science* **2002**, *295*, 469–472.

Scheme 2

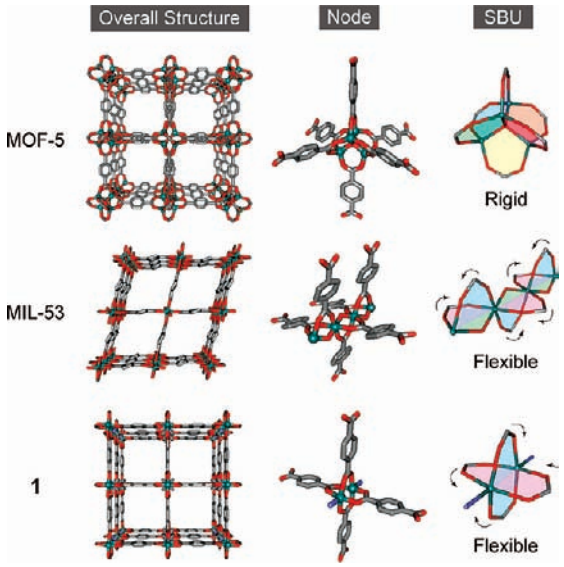

Scheme 3

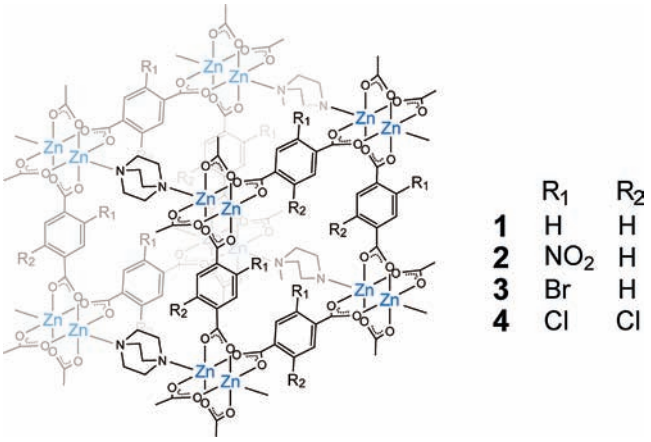

adsorption/desorption,[13a,b] and postsynthetic modified structures also show two-step adsorption for N_2, Ar, and CO_2.[15]

Compound **1** has a jungle-gym-type structure,[5] in which a two-dimensional (2-D) square grid composed of dinuclear Zn_2 units is bridged by dabco molecules to extend the 2-D layers into a three-dimensional (3-D) structure, thus affording wide 7.5 × 7.5 Å^2 open channels, which are large enough to allow the passage of small gas molecules.[5a] The advantageous property pertinent to **1** is the ability to modify pore environments while maintaining the topology of the host framework.[5b] By simply varying the length of the organic linkers, isostructural compounds with a range of pore space can be obtained with the same SBU.[6,13] Although MIL-53 has been thoroughly investigated,[12] compounds that have been systematically evaluated from the standpoint of stepwise adsorption are relatively rare; thus, jungle-gym-type porous coordination polymers would become the next candidates for investigating the breathing effect. Here, we show MeOH, EtOH, IPA, and Me_2CO adsorption on four types of jungle-gym-type porous coordination polymers (Scheme 3), **1**, $[Zn_2(bdc\text{-}NO_2)_2(dabco)]_n$ (**2**, bdc-NO_2 = nitroterephthalate), $[Zn_2(bdc\text{-}Br)_2(dabco)]_n$ (**3**, bdc-Br = bromoterephthalate), and $[Zn_2(bdc\text{-}Cl_2)_2(dabco)]_n$ (**4**, bdc-Cl_2 = 2,5-dichloroterephthalate), to clarify the condition for stepwise adsorption. Varying the adsorbate species, temperature, and bridging ligands in the jungle-gym-type porous coordination polymers, the origin of the stepwise adsorption is discussed in the light of the first adsorption sites.

Experimental Section

Materials. Terephthalic acid was obtained from Aldrich Chemical Co. Zinc nitrate hexahydrate was obtained from Wako Co. Bromoterephthalic acid, nitroterephthalic acid, 2,5-dichloroterephthalic acid, and 1,4-diazabicyclo[2.2.2]octane were obtained from Tokyo Kasei Industrial Co. $[Zn_2(bdc)_2(dabco)]_n$ (**1**) was obtained according to the previous procedure.[5] Compound $\{[Zn_2(bdc\text{-}NO_2)_2(dabco)]\cdot solvents\}_n$ (**2** ⊃ *solvents*) was synthesized according to the previous procedure.[13c]

Synthesis of $\{[Zn_2(bdc\text{-}Br)_2(dabco)]\cdot solvents\}_n$ (3 ⊃ *solvents*). H_2(bdc-Br) (490 mg, 2.0 mmol), $Zn(NO_3)_2\cdot 6H_2O$ (595 mg, 2.0 mmol), and dabco (112 mg, 1.0 mmol) were mixed in dimethylformamide (DMF, 30 mL) and homogenized by stirring for 5 min. The slurry was heated to 120 °C in a Teflon autoclave for 48 h to obtain white crystals. For elemental analysis these crystals were collected and dried in vacuo at 100 °C for 2 h to afford $[Zn_2(bdc\text{-}Br)_2(dabco)]_n$ (**3**) (602 mg, 83%). Elemental analysis calcd for $C_{22}H_{18}Br_2N_2O_8Zn_2$ (728.97): C, 36.25; H, 2.49; N, 3.84. Found: C, 36.37; H, 2.63; N, 3.78.

Synthesis of $\{[Zn_2(bdc\text{-}Cl_2)_2(dabco)]\cdot solvents\}_n$ (4 ⊃ *solvents*). H_2(bdc-Cl_2) (470 mg, 2.0 mmol), $Zn(NO_3)_2\cdot 6H_2O$ (595 mg, 2.0 mmol), and dabco (112 mg, 1.0 mmol) were mixed in DMF (30 mL) and homogenized by stirring for 5 min. The solution was heated to 120 °C in a Teflon autoclave for 48 h to obtain white crystals. For elemental analysis these crystals were collected and dried in vacuo at 140 °C for 1 h to afford $[Zn_2(bdc\text{-}Cl_2)_2(dabco)]_n$ (**4**) (313 mg, 44%). Elemental analysis calcd for $C_{22}H_{16}Cl_4N_2O_8Zn_2$ (708.96): C, 37.27; H, 2.27; N, 3.95. Found: C, 37.75; H, 2.32; N, 3.86.

X-ray Crystal Analysis. Single crystals of **3** ⊃ *solvents* and **4** ⊃ *solvents* were mounted on a glass fiber and coated with epoxy resin. X-ray data collections were carried out using an imaging plate detector of a CCD two-dimensional detector of Rigaku Mercury diffractometer (**3** ⊃ *solvents*) or a Rigaku RAXIS-RAPID diffractometer (**4** ⊃ *solvents*) with graphite monochromated Mo−Kα radiation (λ = 0.7107 Å). For **3** ⊃ *solvents*, the sizes of the unit cells were determined from reflections collected on the setting angles of six frames by changing ω by 0.5° for each frame, and intensity data were collected with a ω scan width of 0.5°. For **4** ⊃ *solvents*, the sizes of the unit cells were determined from reflections collected on the setting angles of three frames by changing ω by 3.0° for each frame, and intensity data were collected with an ω scan width of 5.0°. Two different χ settings were used. Empirical absorption correction[16] was performed for all data. The structures were solved (Table 1) by the direct method with the subsequent difference Fourier syntheses and the refinement with the SHELXTL (version 5.1) software package.[17] The non-hydrogen atoms were refined anisotropically and all hydrogen atoms were placed in the ideal positions. In **3** ⊃ *solvents*, the disordered C5−9 atoms of dabco were isotropically refined. In **4** ⊃ *solvents*, the O5, O6, N2, N3, and C12−17 atoms of DMF molecules were found in final stage, and isotropically refined under the rigid condition. In both **3** ⊃ *solvents* and **4** ⊃ *solvents*, it is impossible to find additional DMF molecules in the framework because of the highly disorders.

Physical Measurements. Thermal gravimetry (TG) was carried out with a Rigaku Instrument TG8120 in a helium flow

(15) Wang, Z.; Cohen, S. M. *J. Am. Chem. Soc.* **2009**, *131*, 16675–16677.

(16) Higashi, T. *Abscor - Empirical Absorption Correction based on Fourier Series Approximation*; Rigaku Corporation: Tokyo, Japan, 1995.

(17) *SHELXTL Reference Manual*, ver. 5.1; Bruker AXS, Analytical X-Ray Systems: Madison, WI, 1997.

Table 1. Crystal Data and Structure Refinements of $\{[Zn_2(bdc\text{-}Br)_2(dabco)]\cdot solvents\}_n$ (**3** ⊃ *solvents*) and $\{[Zn_2(bdc\text{-}Cl_2)_2(dabco)]\cdot solvents\}_n$ (**4** ⊃ *solvents*)

compound	**3** ⊃ *solvents*	**4** ⊃ *solvents*
chemical formula	$C_{11}H_6BrNO_4Zn$	$C_{272}Cl_{32}N_{48}O_{96}Zn_{16}$
formula weight	361.45	7655.52
crystal system	orthorhombic	tetragonal
space group	*Pban*	$I4_1/acd$
temperature [K]	298	298
a [Å]	14.627(3)	21.818(3)
b [Å]	16.176(3)	21.818(3)
c [Å]	9.6414(19)	38.660(8)
α [deg]	90	90
β [deg]	90	90
γ [deg]	90	90
V [Å^3]	2281.1(8)	18402(5)
Z	4	2
D_c [g cm^{-1}]	1.052	1.382
μ (MoKα) [mm^{-1}]	2.830	1.333
2θ range [deg]	6.6−55.0	6.3−55.0
GOF on F^2	1.332	1.039
$R_1{}^a$ [$I > 2.0\sigma(I)$]	0.1057	0.0779
$wR_2{}^b$ [all data]	0.3831	0.2415

$^a R_1 = \sum(|F_o| - |F_c|)/\sum(|F_o|)$. $^b wR_2 = \{\sum[w(F_o^2 - F_c^2)^2]/\sum[w(F_o^2)^2]\}^{1/2}$.

(100 mL/min) with heating rate of 10 K/min. Differential scanning calorimetry (DSC) was carried out with a Rigaku Instrument TG8230 in a nitrogen flow (70 mL/min) with heating rate of 20 K/min, and the heats of desorption were calibrated by melting high-purity indium, lead, and antimony. IR spectra were recorded on a JASCO FT/IR-610 spectrophotometer with samples prepared with KBr. X-ray powder diffraction (XRPD) data were collected on a Rigaku RINT-2200YS diffractometer with CuKα radiation. N_2 (77 K) adsorption measurement was carried out in Quantachrome Autsorb-1. The adsorption isotherms of gaseous MeOH, EtOH, *i*-PrOH, and Me_2CO were measured by using BELSORP18-Plus volumetric adsorption equipment from BEL JAPAN. The saturated vapor pressures were calculated using the following equation, $\log_{10}P = A - B/(T + C)$, where P is the saturated vapor pressure (Torr), T is the temperature in degrees Celsius, and A, B, and C are constants defined by the adsorbate. MeOH: $A = 8.07246$, $B = 1574.99$, $C = 238.86$; EtOH: $A = 8.21337$, $B = 1652.05$, $C = 231.48$; *i*-PrOH: $A = 8.39424$, $B = 1730.00$, $C = 231.45$; Me_2CO: $A = 7.23967$, $B = 1279.87$, $C = 237.5$.

Results and Discussion

***i*-PrOH, EtOH, and Me_2CO Adsorption/Desorption on $[Zn_2(bdc)_2(dabco)]$ (1).** As reported previously, *i*-PrOH (IPA) adsorption/desorption on **1** shows a two-step profile (Supporting Information, Figure S1a).[13a,b] The IPA adsorption process involves the intermediate state $\{[Zn_2(bdc)_2(dabco)]\cdot 3IPA\}_n$ (**1** ⊃ 3IPA), in which the framework is highly shrunk with loading of three IPA molecules per pore, compared with empty or filled frameworks.[13a] This shrinkage produces a slowing down of the adsorption kinetics, and then a further increase in the adsorption pressure after the threshold pressure ($P_{th,ad}$) leads to a reopening of the total porosity and complete pore filling (eq 1).

$$\mathbf{1} + 4.5\text{IPA} \rightleftarrows \mathbf{1}\supset 3\text{IPA} + 1.5\text{IPA} \rightleftarrows \mathbf{1}\supset 4.5\text{IPA} \qquad (1)$$

A similar stepwise adsorption is observed in the MeOH and EtOH adsorption isotherms on **1** (Supporting Information, Figures S1b and S1c).[13b] In contrast, Me_2CO adsorption on **1** shows a single step, indicative of a typical type-I isotherm (Supporting Information, Figure S1d), where Me_2CO micropore filling occurs in the very low P/P_0 region.[13b] Saturated Me_2CO amounts are about 5.0 molecules per Zn_2,

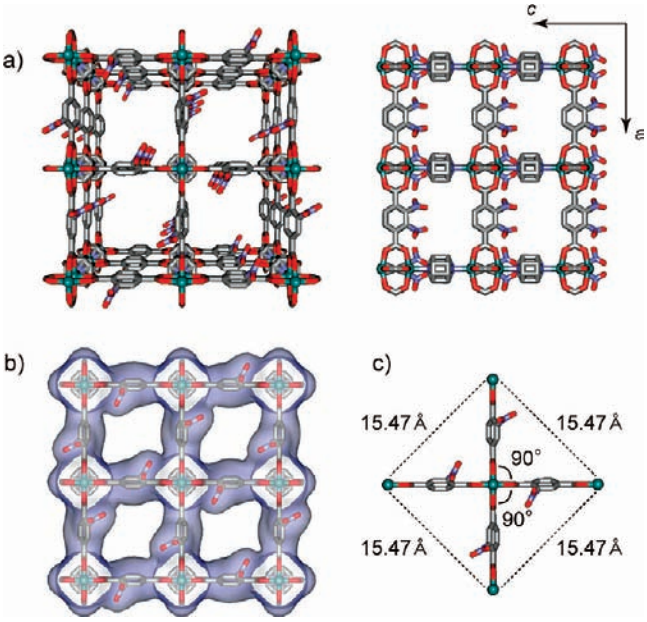

Figure 1. (a) Crystal structures of $[Zn_2(bdc\text{-}NO_2)_2(dabco)]_n$ (**2**). (b) Space-filling structures of **2** along the *c* axis. (c) Amplified view around the Zn_2 moiety with selected distances and angles.

at which $\{[Zn_2(bdc)_2(dabco)]\cdot 5Me_2CO\}_n$ (**1** ⊃ $5Me_2CO$) is produced. As the adsorbate molecular sizes decrease (IPA > Me_2CO > EtOH > MeOH), the saturated amounts increase: 4.5 (IPA), 5.0 (Me_2CO), 6.0 (EtOH), and 8.0 (MeOH) molecules per pore.[18] Considering that alcohol adsorption isotherms are two-step profiles but those of Me_2CO are not, it could be concluded that hydrogen bonds are involved in the two-step adsorption on jungle-gym-type porous coordination polymers. As found in the IPA adsorption process,[13a] two-step adsorption is attributed to the highly shrunk intermediate state. Consequently, MeOH and EtOH molecules are also adsorbed via the shrunk intermediate state, which is produced by the hydrogen bonds. The remaining problem is how hydrogen bonds form in the pores, and it is possible to obtain detailed information using isomorphous frameworks, the results of which are shown in the next paragraph.

Syntheses and Crystal Structures of 2 ⊃ *solvents*, 3 ⊃ *solvents*, and 4 ⊃ *solvents*. The advantageous property pertinent to the jungle-gym-type porous coordination polymers is the ability to modify pore environments while maintaining the topology of the host framework.[5b] To monitor the differences in adsorption behaviors under the same conditions, we set out to vary the dicarboxylate ligands (bdc) in the original framework **1** without altering the overall connectivity of the nets. Dicarboxylate linkers with bdc-NO_2, bdc-Br, and bdc-Cl_2 were used instead of bdc in **1**, which resulted in a series of isomorphous frameworks, $\{[Zn_2(bdc\text{-}NO_2)_2(dabco)]\cdot solvents\}_n$ (**2** ⊃ *solvents*), $\{[Zn_2(bdc\text{-}Br)_2(dabco)]\cdot solvents\}_n$ (**3** ⊃ *solvents*), and $\{[Zn_2(bdc\text{-}Cl_2)_2(dabco)]\cdot solvents\}_n$ (**4** ⊃ *solvents*). Figures 1−3 show the results of single-crystal X-ray analyses for **2**,[19] **3** ⊃ *solvents*,

(18) Strictly speaking, integer values are not proper for adsorption amounts because adsorption is a continuous process. However, it is valid to use in the comparison of adsorption amounts among several adsobate-absorbent systems. Hereafter, all adsorption amounts are made in this way.

(19) Single crystals of **2** ⊃ *solvents* keep their crystalline form without guest molecules, which was checked by single-crystal X-ray analysis. Single-crystal X-ray analysis, TG, XRPD, and N_2 adsorption measurements for **2** are reported in reference 13c.

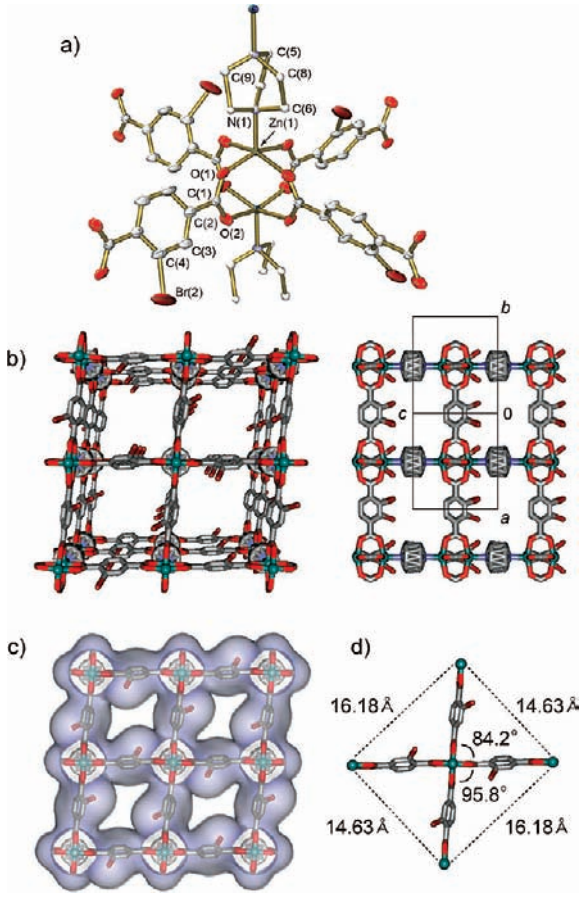

Figure 2. (a) ORTEP drawing of $\{[Zn_2(bdc\text{-}Br)_2(dabco)]\cdot solvents\}_n$ (**3** ⊃ *solvents*) around Zn_2 at the 30% probability level. Hydrogen atoms, bromo moieties, and carbon atoms at dabco with disorder relationship are omitted for clarity. (b) Crystal structures of **3** ⊃ *solvents*. (c) Space-filling structures of **3** ⊃ *solvents* along the *c* axis. (d) Amplified view around the Zn_2 moiety with selected distances and angles.

and **4** ⊃ *solvents*, respectively. The primary building unit in all three compounds is a well-known binuclear "paddle-wheel" zinc carboxylate complex, where these Zn_2 units are connected in 2-D via rigid dicarboxylic bridges into infinite planar layers having a grid topology. Axially coordinated dabco ligands to Zn_2 units link each layer along the *c*-axis, affording a porous 3-D net with tetragonal (distorted cubic) structure. Considering the van der Waals radii for the constituent atoms, the free sizes of the intersecting channels along the *c*-axis vary from 6.2 × 4.3 Å^2 for **2** to 5.0 × 2.0 Å^2 for **3** ⊃ *solvents*, and 3.8 × 3.8 Å^2 for **4** ⊃ *solvents*. In **2**, the nitro moieties are oriented to the pore with a 65.9° inclination to the benzene plane, and the dihedral angles of the benzene rings are inclined (20.0°) to the channel direction along the *c*-axis. Also in both **3** ⊃ *solvents* and **4** ⊃ *solvents*, the Br and Cl moieties stick out from the pores with the benzene inclined to the channel (26.0° and 23.1°, respectively). The calculated guest-accessible free volumes for frameworks **2**−**4** were found to be 27, 44, and 57%, respectively.[20] The inner microporous space of the as-prepared hosts is occupied by guest solvent DMF molecules; however, we were not able to locate these guest molecules in **3** ⊃ *solvents* and **4** ⊃ *solvents* because of the high crystal symmetry and intrinsic disorder.

(20) Speck, A. L. *A. M. C. T. PLATON*; Utrecht University: Utrecht, The Netherlands, 1999.

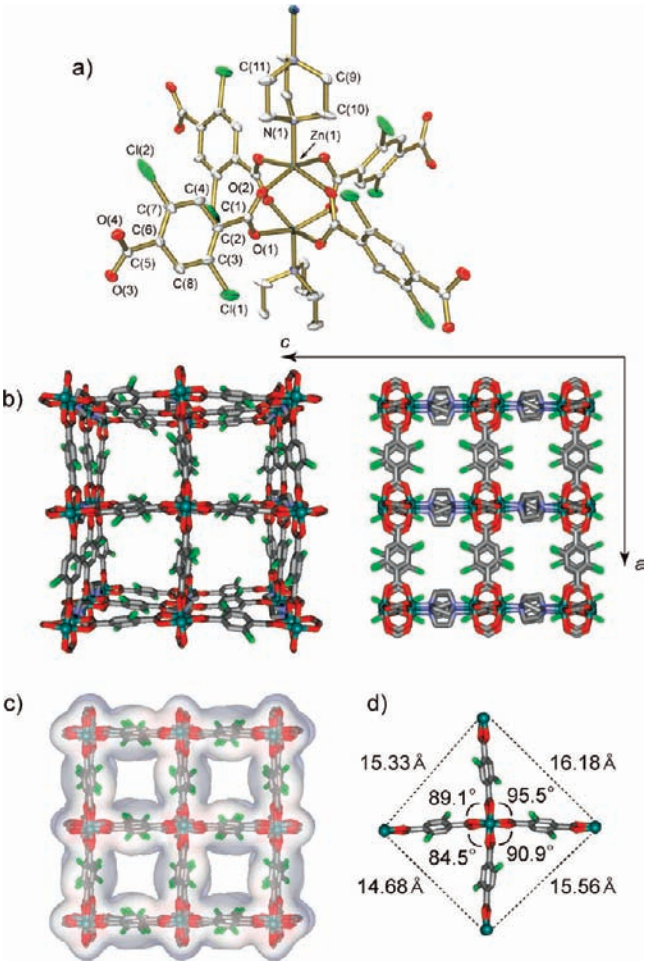

Figure 3. (a) ORTEP drawing of $\{[Zn_2(bdc\text{-}Cl_2)_2(dabco)]\cdot solvents\}_n$ (**4** ⊃ *solvents*) around Zn_2 at the 30% probability level. Hydrogen atoms and DMF molecules are omitted for clarity. (b) Crystal structures of **4** ⊃ *solvents*. (c) Space-filling structures of **4** ⊃ *solvents* along the *c* axis. (d) Amplified view around the Zn_2 moiety with selected distances and angles.

Interestingly, the layer stacking modes in **2**, **3** ⊃ *solvents*, and **4** ⊃ *solvents* are different. In **2** and **3** ⊃ *solvents*, the layers of $[Zn_2(COO)_4N_2]$ are situated exactly on top of each other and hence form AAAA-type packing, where **2** has a square section like $[Zn_2(bdc)_2(dabco)]_n$ (**1**),[5a] and **3** ⊃ *solvents* has a rhomboid section like $\{[Zn_2(bdc)_2(dabco)]\cdot 2C_6H_6\}_n$ (**1** ⊃ $2C_6H_6$).[5a] In contrast, in **4** ⊃ *solvents*, the undulating layers alternate obeying an ABAB law, like $\{[Zn_2(bdc)_2(dabco)]\cdot 4DMF\cdot 1/2H_2O\}_n$ (**1** ⊃ $4DMF\cdot 1/2H_2O$),[5a] as shown in Figure 3b. This difference in the layer stacking modes is attributed to the framework flexibilities mainly originating from the variety of coordination modes around the Zn_2 units. Figures 1c, 2d, and 3d show the three types of coordination modes around the Zn_2 units found in **2**, **3** ⊃ *solvents*, and **4** ⊃ *solvents*, respectively. In **2**, mutually perpendicular coordination bonds (type-α) afford square cross-sectional pores, whereas in **3** ⊃ *solvents*, rhomboid cross-sectional pores are produced by inclination of coordination bonds to one another (type-β) with angles of 84.2°. In contrast, in **4** ⊃ *solvents*, the coordination is asymmetrically distorted (type-γ): all angles among the coordination bonds are different (95.5°, 90.9°, 84.5°, and 89.1°).

Table 2 summarizes the jungle-gym-type porous coordination polymers containing dabco ligands, which are classified into three types of coordination mode (type-α, -β, and -γ)

Table 2. Selected Jungle-Gym-Type Porous Coordination Polymers Containing Dabco Ligands[a]

compound	coordination mode	reference
$\{[Cu_2(tfbdc)_2(dabco)]\cdot solvents\}_n$	type-α	6c
$\{[Co_2(bodc)_2(dabco)]\cdot 3.5DMF\}_n$	type-α	6l
$[Zn_2(bdc)_2(dabco)]_n$ (**1**)	type-α	5a
$\{[Zn_2(bdc)_2(dabco)]\cdot 4DMF\cdot 1/2H_2O\}_n$ (**1** ⊃ $4DMF\cdot 1/2H_2O$)	type-α	5a
$\{[Zn_2(bdc)_2(dabco)]\cdot 4.5IPA\}_n$ (**1** ⊃ 4.5IPA)	type-α	13a
$\{[Zn_2(bdc)_2(dabco)]\cdot 2C_6H_6\}_n$ (**1** ⊃ $2C_6H_6$)	type-β	5a
$\{[Zn_2(tmbdc)_2(dabco)]\cdot solvents\}_n$	type-α	5b
$[Zn_2(ndc)_2(dabco)]_n$	type-α	5b
$[Zn_2(tfbdc)_2(dabco)]_n$	type-α	5b
$[Zn_2(bdc\text{-}NO_2)_2(dabco)]_n$ (**2**)	type-α	13c
$\{[Zn_2(adc)_2(dabco)]\cdot solvents\}_n$	type-α	6h
$\{[Zn_2(camph)_2(dabco)]\cdot DMF\cdot H_2O\}_n$	type-α	6j
$\{[Zn_2(bdc\text{-}Br)_2(dabco)]\cdot solvents\}_n$ (**3** ⊃ *solvents*)	type-β	this work
$\{[Zn_2(bdc\text{-}Cl_2)_2(dabco)]\cdot solvents\}_n$ (**4** ⊃ *solvents*)	type-γ	this work

[a] dabco = 1,4-diazabicyclo[2.2.2]octane, H_2tfbdc = tetrafluorobenzene-1,4-dicarboxylic acid, H_2bodc = bicyclo[2.2.2]octane-1,4-dicarboxylic acid, H_2bdc = 1,4-benzenedicarboxylic acid, H_2tmbdc = tetramethylterephthalic acid, H_2ndc = 1,4-naphthalenedicarboxylic acid, H_2(bdc-NO_2) = nitroterephthalic acid, H_2adc = 9,10-anthracenedicarboxylic acid, H_2camph = (+)-camphoric acid, H_2(bdc-Br) = bromoterephthalic acid, H_2(bdc-Cl_2) = 2,5-dichloroterephthalic acid.

according to the definition given above. The trend is found that type-α is favored when symmetrical dicarboxylate ligands are coordinated to the Zn_2 units. A noteworthy success is that all these three types of coordination mode are constructed with the introduction of substitution into **1**, in **2**, **3** ⊃ *solvents*, and **4** ⊃ *solvents*, respectively. It is possible for **1** to have two types of coordination modes, type-α and type-β, responding to the guest species.[5a] As reported previously,[13a] the intermediate **1** ⊃ 3IPA is type-β, where two states originating from type-α and type-β go back and forth between the counterparts.

Thermal Stabilities and Porosities of 2−4. Supporting Information, Figure S2 shows the thermograms of **2** ⊃ *solvents*, **3** ⊃ *solvents*, and **4** ⊃ *solvents* in the temperature range 20−300 °C for a heating rate β = 10 °C/min. In the temperature range 20−200 °C, the thermograms of **2** ⊃ *solvents* and **3** ⊃ *solvents* showed a mass loss (observed = 30.0% and 30.4%, respectively) corresponding to guest molecules. In contrast, the thermogram of **4** ⊃ *solvents* showed a two-step loss in the temperature range of 20−78 °C (observed = 32.3%) and 78−180 °C (observed = 19.7%), which correspond to surface-adsorbed molecules and guest molecules, respectively. On the assumption that all guests are DMF, 3.9, 4.4, and 4.0 molecules are adsorbed in one pore of **2** ⊃ *solvents*, **3** ⊃ *solvents*, and **4** ⊃ *solvents*, respectively. All **2** ⊃ *solvents*, **3** ⊃ *solvents*, and **4** ⊃ *solvents* were readily desolvated to give $[Zn_2(bdc\text{-}NO_2)_2(dabco)]_n$ (**2**), $[Zn_2(bdc\text{-}Br)_2(dabco)]_n$ (**3**), and $[Zn_2(bdc\text{-}Cl_2)_2(dabco)]_n$ (**4**) by drying in vacuo at 120 °C for 3 h, at 100 °C for 2 h, and 140 °C for 1 h (Supporting Information, Figure S2b, d, and f), respectively. As shown in Figure 4, the XRPD patterns of **2**, **3**, and **4** show sharp peaks at similar peak positions corresponding to the as-prepared compounds, indicating that compounds **2**, **3**, and **4** maintain their frameworks after removal of the guest molecules.

Figure 5 shows the results of N_2 adsorption/desorption experiments conducted on **2**−**4** at 77 K. The adsorption isotherms display type-I curves, corresponding to apparent

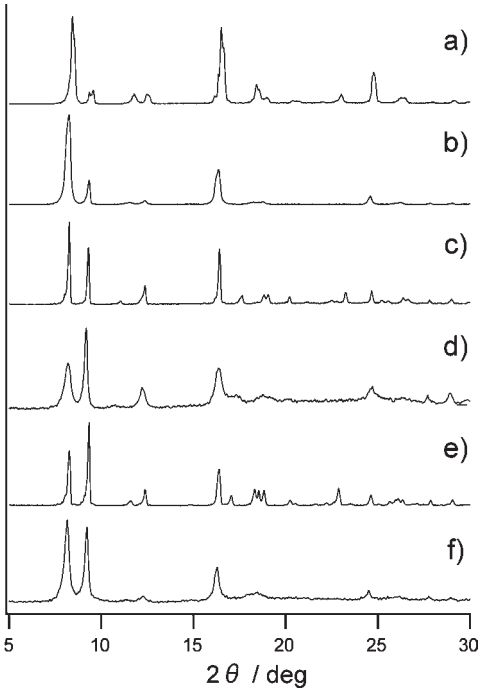

Figure 4. XRPD patterns of (a) $\{[Zn_2(bdc\text{-}NO_2)_2(dabco)]\cdot solvents\}_n$ (**2** ⊃ *solvents*), (b) dried **2** ⊃ *solvents* at 120 °C for 3 h (= **2**), (c) $\{[Zn_2(bdc\text{-}Br)_2(dabco)]\cdot solvents\}_n$ (**3** ⊃ *solvents*), (d) dried **3** ⊃ *solvents* at 100 °C for 2 h (= **3**), (e) $\{[Zn_2(bdc\text{-}Cl_2)_2(dabco)]\cdot solvents\}_n$ (**4** ⊃ *solvents*), and (f) dried **4** ⊃ *solvents* at 140 °C for 1 h (= **4**).

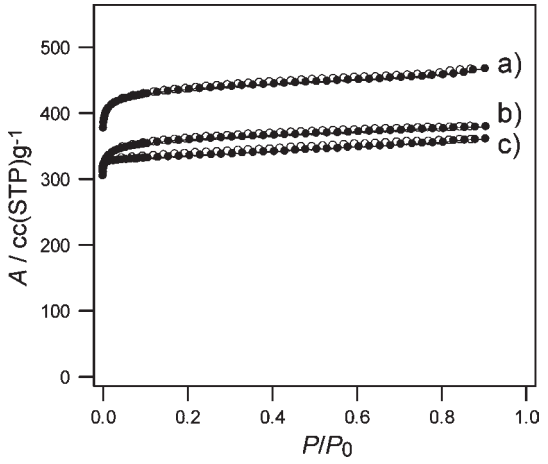

Figure 5. Isotherm for N_2 adsorption (filled circles) and desorption (open circles) at 77 K of (a) $[Zn_2(bdc\text{-}NO_2)_2(dabco)]_n$ (**2**), (b) $[Zn_2(bdc\text{-}Br)_2(dabco)]_n$ (**3**), and (c) $[Zn_2(bdc\text{-}Cl_2)_2(dabco)]_n$ (**4**). P_0 is a saturated vapor pressure of N_2 at 77 K.

Table 3. Summary of N_2 Gas Adsorption on **1**−**4**

compound	BET surface area ($m^2\ g^{-1}$)	Langmuir surface area ($m^2\ g^{-1}$)	N_2 per pore
1	1450 [a]	2090 [a]	12.3 [a]
2	1568	2000	10.6
3	1292	1642	9.7
4	1216	1545	8.8

[a] Data was reported in ref 5b.

Brunauer−Emmett−Teller (BET) and Langmuir surface areas, as shown in Table 3. Despite the bulky substitution in **2**, the surface area of **2** is comparable to that of **1**. N_2 adsorption amounts on **2**−**4** are 10.6 (**2**), 9.7 (**3**), and 8.8 (**4**)

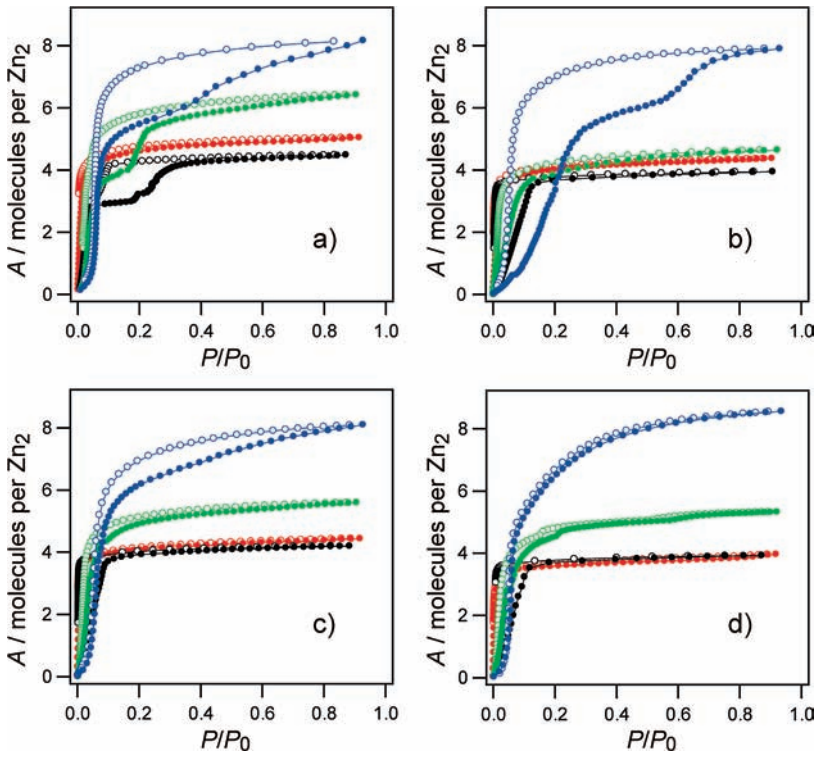

Figure 6. Isotherms for vapor adsorption (filled circles) and desorption (open circles) of MeOH (blue), EtOH (green), *i*-PrOH (black), and Me_2CO (red) on (a) $[Zn_2(bdc)_2(dabco)]_n$ (**1**), (b) $[Zn_2(bdc\text{-}NO_2)_2(dabco)]_n$ (**2**), (c) $[Zn_2(bdc\text{-}Br)_2(dabco)]_n$ (**3**), and (d) $[Zn_2(bdc\text{-}Cl_2)_2(dabco)]_n$ (**4**) at 298 K over the relative pressure range from 0 to 0.9 (P_0 is the saturated vapor pressure). EtOH isotherms on **3** and **4** were measured at 308 and 318 K, respectively. The results of **1** were shown in a previous report, ref 13b.

molecules per pore, which are comparable to other jungle-gym-type porous coordination polymers,[5b] 9.9 for $[Zn_2(tmbdc)_2(dabco)]_n$ (tmbdc = tetramethylterephthalate) and 11.9 for $[Zn_2(tfbdc)_2(dabco)]_n$ (tfbdc = tetrafluoroterephthalate). These results also supports the pore stabilities of **2**−**4** without guest molecules.

Vapor Adsorption/Desorption Isotherms on 1−**4.** Figure 6 shows MeOH, EtOH, IPA, and Me_2CO adsorption/desorption isotherms on **1**−**4**. Following the order of molecular sizes, compounds **1**−**4** adsorb each adsorbate with saturated amounts of MeOH > EtOH > Me_2CO ≥ IPA. XRPD patterns of **2**−**4** exposed to each of the solvent vapors show intense peaks with similar positions (Supporting Information, Figure S6−8), indicating that **2** − **4** adsorb vapors without framework collapse.[21] As well as **1**, Me_2CO adsorption isotherms on **2**− **4** exhibit type-I isotherms and show no apparent hysteresis. In contrast, almost all alcohol vapor isotherms show hysteresis loops. In **2** − **4**, the most remarkable feature is that a clear two-step isotherm is only observed in MeOH adsorption on **2** (a substep isotherm is observed in MeOH adsorption on **3**). Although the larger sizes of EtOH and IPA adsorption on **1** exhibit clear two-step isotherms (Figure 6a), those on **2** − **4** show single-step isotherms.

The characteristic curve using the Polanyi adsorption potential ($= RT \ln(P_0/P)$) displays adsorption data at low pressures much better and demonstrates clearly the difference in the affinity for the adsorbates.[6k] Comparisons of characteristic adsorption curves corresponding to those in Figure 6 are shown in Figure 7. All compounds adsorb Me_2CO in higher affinity regions in conformity with sharp uptakes at lower relative pressures, which may be attributed to the π affinities with the internal benzene rings of the frameworks. In contrast, alcohol molecules are adsorbed at lower regions of $RT \ln(P_0/P)$, because jungle-gym-type porous coordination polymers **1**−**4** have less hydrophilic pores. Such a logarithmic plot for the MeOH isotherm on **2** also shows an apparent two-step profile, as well as the alcohol isotherms on **1**.

Although the information about first adsorption sites of MeOH on both **1** and **2** would set the stage for the origin of the two-step adsorption, observations by single-crystal X-ray analyses are difficult because of the high crystallographic symmetry. However, on the assumption that the molecules are mostly adsorbed near the corners of the cavities,[22] the first adsorption site of MeOH is presumed to be the corner around the carboxylate groups of bdc (or bdc-NO_2) ligands. This hypothesis is supported by previous reports[23] on molecule adsorption sites in **1**, where methane and hydrogen adsorption sites were determined by in situ single-crystal X-ray crystallography and calculation, respectively. Both results show that parts of the first adsorption sites form the corner around the carboxylate groups of the bdc ligands. Furthermore, it is valid to consider that penetrated hydrophilic MeOH molecules are far apart from hydrophobic spaces afforded by the internal benzene rings, and brought so close to the carboxylate groups with hydrogen bonds. Therefore, it seems reasonable to assume that such a formation

(21) XRPD patterns of **1** exposed to each solvent vapor are shown in reference 13b, also indicating that **1** adsorbs vapors without framework collapses.

(22) Walton, K. S.; Millward, A. R.; Dubbeldam, D.; Frost, H.; Low, J. J.; Yaghi, O. M.; Snurr, R. Q. *J. Am. Chem. Soc.* **2008**, *130*, 406–407.

(23) (a) Kim, H.; Samsonenko, D. G.; Das, S.; Kim, G.-H.; Lee, H.-S.; Dybtsev, D. N.; Berdonosova, E. A.; Kim, K. *Chem. Asian J.* **2009**, *4*, 886–891. (b) Nijem, N.; Veyan, J.-F.; Kong, L.; Li, K.; Pramanik, S.; Zhao, Y.; Li, J.; Langreth, D.; Chabal, Y. J. *J. Am. Chem. Soc.* **2010**, *132*, 1654–1664.

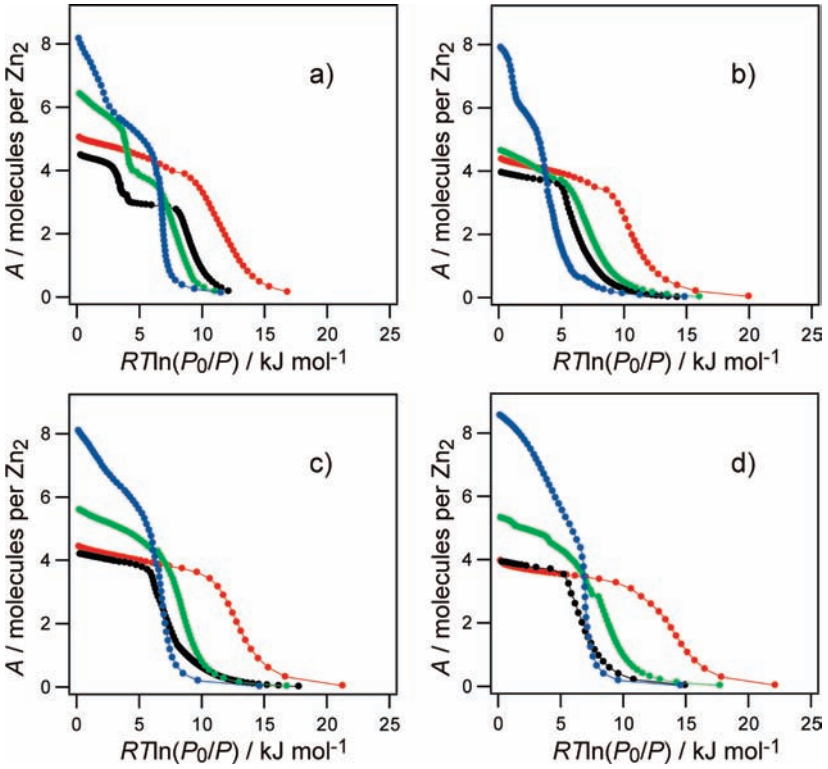

Figure 7. Characteristic adsorption curves of MeOH (blue), EtOH (green), *i*-PrOH (black), and Me_2CO (red) on (a) $[Zn_2(bdc)_2(dabco)]_n$ (**1**), (b) $[Zn_2(bdc\text{-}NO_2)_2(dabco)]_n$ (**2**), (c) $[Zn_2(bdc\text{-}Br)_2(dabco)]_n$ (**3**), and (d) $[Zn_2(bdc\text{-}Cl_2)_2(dabco)]_n$ (**4**) at 298 K over the relative pressure range from 0 to 0.9 (P_0 is the saturated vapor pressure). EtOH isotherms on **3** and **4** were measured at 308 and 318 K, respectively.

of hydrogen bonds between the carboxylate groups and guest molecules produces the shrunk frameworks, being the origin of the two-step adsorption (Supporting Information, Figure S9). Undoubtedly, under conditions that hinder such formation of a hydrogen bond by introducing substitution ($-NO_2$, $-Br$, $-Cl$) as obstacles around the corner, or using bulky alcohols making it hard to penetrate into the corner, the two-step adsorption is not observed.

Thermal Analyses of Two-Step Adsorption Isotherms on 1. To fully understand the difference, the mechanisms of *i*-PrOH, EtOH, and Me_2CO adsorption/desorption on **1** were pursued by thermal analyses. Figures 8 and S11 show adsorption/desorption isotherms for EtOH and Me_2CO at various temperatures, respectively. Each EtOH adsorption isotherm shows a sharp increase at low relative pressures and then assumes the plateau form to be $\{[Zn_2(bdc)_2(dabco)]\cdot 4EtOH\}_n$ (**1** ⊃ 4EtOH). After reaching $P_{th,ad}$ (0.73 (288), 1.29 (298), 1.81 (308), 2.94 (318), and 4.55 kPa (328 K)), the curve exhibits another gradual increase and finally attains a saturated level at which $\{[Zn_2(bdc)_2(dabco)]\cdot 6EtOH\}_n$ (**1** ⊃ 6EtOH) is produced. In both EtOH and Me_2CO adsorption isotherms, the saturated amounts do not vary over the measured temperatures, that is, without collapsing the framework **1** adsorbs EtOH and Me_2CO with a similar adsorption mechanism in those temperature regions, affording **1** ⊃ 6EtOH via **1** ⊃ 4EtOH, and **1** ⊃ $5Me_2CO$, as expressed in eqs 2 and 3,

$$\mathbf{1} + 6\text{EtOH} \rightleftarrows \mathbf{1}\supset 4\text{EtOH} + 2\text{EtOH} \rightleftarrows \mathbf{1}\supset 6\text{EtOH} \quad (2)$$

$$\mathbf{1} + 5Me_2CO \rightleftarrows \mathbf{1}\supset 5Me_2CO \quad (3)$$

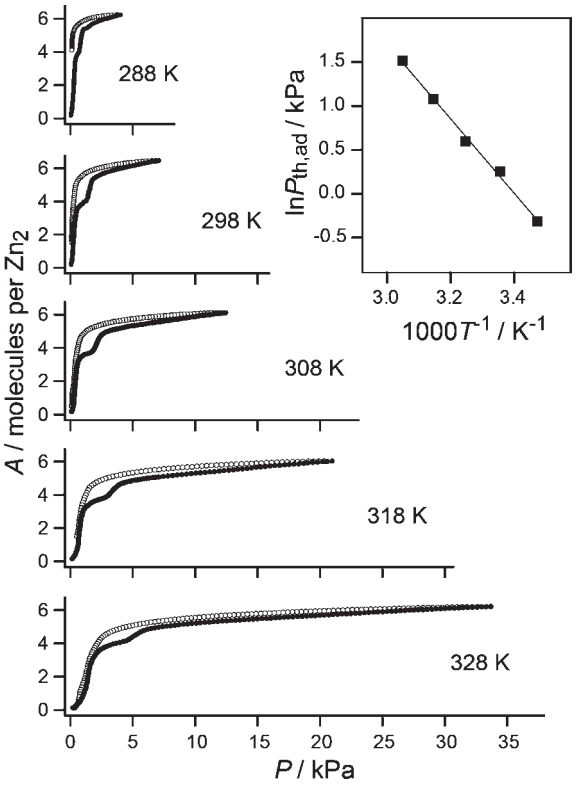

Figure 8. Isotherms (left) of the vapor adsorption (filled circle) and desorption (open circle) of EtOH on $[Zn_2(bdc)_2(dabco)]_n$ (**1**) at 288, 298, 308, 318, and 328 K. The saturated vapor pressure; EtOH: 4.321 kPa (at 288 K), 7.887 kPa (at 298 K), 13.761 kPa (at 308 K), 23.061 kPa (at 318 K), 37.277 kPa (328 K). Plots (right) of $\ln P_{th,ad}$ against T^{-1} observed in EtOH adsorption isotherms on **1**.

as well as the temperature dependence in IPA adsorption isotherms, $P_{th,ad}$ found in EtOH adsorption increases with an increase in the temperature (Table 4).[13a] Because $P_{th,ad}$ can be regarded as the equilibrium pressure for EtOH inclusion,[10e,h,11b,13a] its temperature dependence allows us to evaluate the adsorption enthalpy for the EtOH adsorption process based on the Clausius−Clapeyron equation.[24]

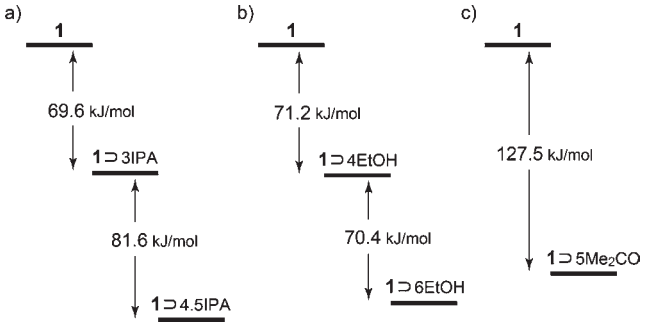

Figure 9. Schematic energy diagram for the solid−gas complexation of **1** with gaseous *i*-PrOH (IPA), EtOH, and Me_2CO.

Table 4. Threshold Pressures ($P_{th,ad}$, kPa) Observed in Vapor Adsorption Isotherms on **1**

	$P_{th,ad}$ (kPa)	
temperature (K)	*i*-PrOH adsorption	EtOH adsorption
288	0.51	0.73
298	1.08	1.29
308	2.13	1.81
318	4.24	2.94
328	8.12	4.55

This relation can be applied to the $P_{th,ad}$ of the adsorption process, thereby showing a linear relationship between the logarithm of $P_{th,ad}$ and the reciprocal of the measurement temperature (Figure 8). The adsorption enthalpy for the second EtOH adsorption (that is, for the process **1** ⊃ 4EtOH + 2EtOH → **1** ⊃ 6EtOH) is $\Delta H_{ad,2}$ (EtOH) = −70.4 kJ mol^{-1}, which is relatively smaller than that in **1** ⊃ 3IPA + 1.5IPA → **1** ⊃ 4.5IPA ($\Delta H_{ad,2}$ (IPA) = −81.6 kJ mol^{-1}).[13a] Considering the vaporization enthalpy of ΔH_{vap} (EtOH) = 42.32 kJ mol^{-1} and ΔH_{vap} (Me_2CO) = 30.99 kJ mol^{-1},[25] the total adsorption enthalpies were estimated by differential scanning calorimetry (DSC) measurements for **1** ⊃ 6EtOH and **1** ⊃ 5Me_2CO: ΔH_{ad} (EtOH) = −141.6 kJ mol^{-1} and ΔH_{ad} (Me_2CO) = −127.5 kJ mol^{-1}.

Figure 9 summarizes the energy diagrams of the IPA, EtOH, and Me_2CO adsorption processes on **1**.[26] The total adsorption enthalpy of Me_2CO is slightly smaller than those of IPA (ΔH_{ad} (IPA) = −151.2 kJ mol^{-1}) and EtOH, because Me_2O adsorption does not involve hydrogen bonds, which supports the claim that alcohol adsorption on **1** involve the formation of hydrogen bonds. Comparing IPA and EtOH adsorption on **1**, the value of the first adsorption enthalpy for EtOH is comparable to that for IPA: $\Delta H_{ad,1}$ (IPA) = −69.6 kJ mol^{-1} and $\Delta H_{ad,1}$ (EtOH) = −71.2 kJ mol^{-1}, indicating that both adsorptions proceed via the shrunk intermediate state, that is, a wide → narrow → wide pore transition has occurred. Although the two-step profile in EtOH adsorption on **1** is relatively ambiguous compared with those of IPA, from an energetic point of view, similar framework transformations are produced. Only focusing on the framework deformations, the energy balances are exothermic in the wide → narrow and endothermic in the

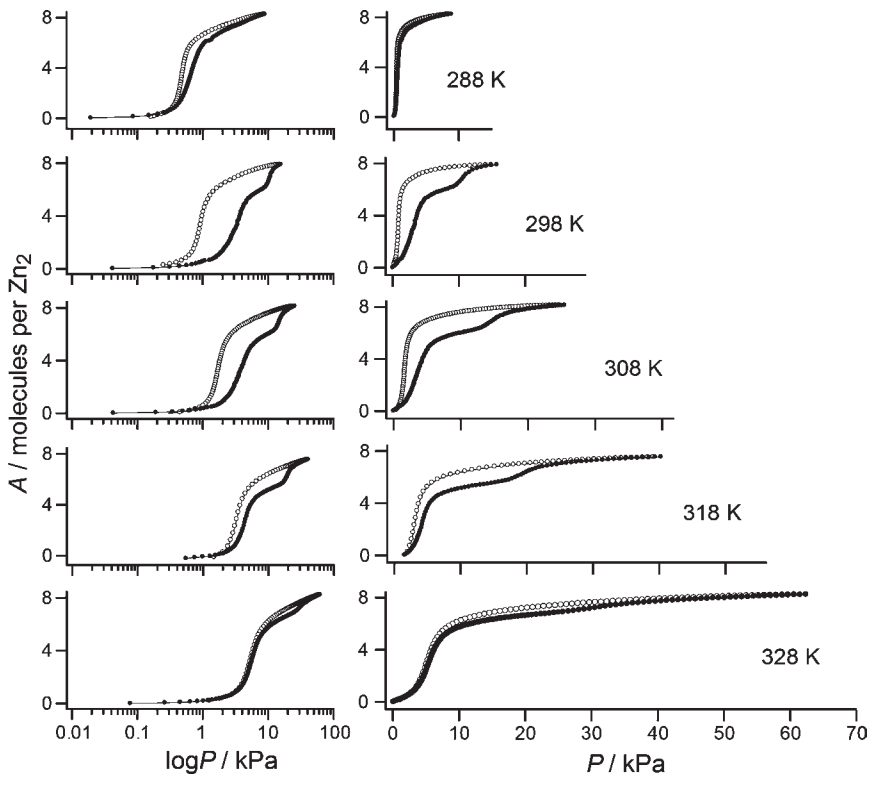

Figure 10. Isotherms for vapor adsorption (filled circles) and desorption (open circles) of MeOH on $[Zn_2(bdc\text{-}NO_2)_2(dabco)]_n$ (**2**) at 288, 298, 308, 318, and 328 K, against log *P* (left) and *P* (right). The saturated vapor pressure; MeOH: 9.842 kPa (at 288 K), 16.913 kPa (at 298 K), 27.937 kPa (at 308 K), 44.543 kPa (at 318 K), 68.801 kPa (328 K).

narrow → wide transitions; however, both second adsorption enthalpies are relatively large. The reason is that in the second adsorption processes hydrogen bonds are reformed among the adsorbate molecules with the realignment (Supporting Information, Figure S9).

Temperature Dependence of Two-Step MeOH Adsorption Isotherm on 2. As mentioned previously, the MeOH adsorption isotherm on **2** at 298 K clearly shows a two-step profile. At 298 K, the MeOH adsorption isotherm shows a gradual increase at low pressures and then assumes the plateau form to be $\{[Zn_2(bdc\text{-}NO_2)_2(dabco)]\cdot 6MeOH\}_n$ (**2** ⊃ 6MeOH). After reaching $P_{th,ad}$ (9.21 kPa), the curve exhibits another gradual increase and finally attains a saturated level at which $\{[Zn_2(bdc\text{-}NO_2)_2(dabco)]\cdot 8MeOH\}_n$ (**2** ⊃ 8MeOH) is produced, as expressed in eq 4.

$$\mathbf{2} + 8\text{MeOH} \rightleftarrows \mathbf{2}\supset 6\text{MeOH} + 2\text{MeOH} \rightleftarrows \mathbf{2}\supset 8\text{MeOH} \quad (4)$$

This two-step profile would also be attributed to the shrunk framework of **2** ⊃ 6MeOH produced by the hydrogen bonds between MeOH molecules and carboxylate groups of the framework.

Figure 10 shows MeOH adsorption/desorption isotherms on **2** at 288, 298, 308, 318, and 328 K. At 288 K, the adsorption/desorption isotherm shows a single-step profile with narrower hysteresis loop. Taking into account that the saturated amounts are 8.0 molecules per pore, **2** adsorbs MeOH to be **2** ⊃ 8MeOH without a pathway of **2** ⊃ 6MeOH, as expressed in eq 5.

$$\mathbf{2} + 8\text{MeOH} \rightleftarrows \mathbf{2}\supset 8\text{MeOH} \quad (5)$$

As the temperature is raised, the width of hysteresis loop becomes narrower with the higher shift of $P_{th,ad}$ (13.06 (308), 17.36 (318), and 25.69 kPa (328 K)), and the step in the adsorption isotherm at 328 K is ambiguous. Those trends are obviously observed in the logarithm plots of adsorption isotherms (Figure 10 left). Thus, there is a temperature dependence (298−318 K) for the appearance of two-step profiles in MeOH adsorption on **2**, which also supports the claim that the formation of hydrogen bonds between the carboxylate groups and guest molecules producing the shrunk frameworks is the origin of the two-step adsorption. Above 318 K, it is hard to form hydrogen bonds between MeOH molecules and carboxylate groups, because the formation is exothermic. In contrast, in the case below 298 K, the hydrogen-bond formation may be hindered by another formation between $-NO_2$ moieties and MeOH molecules. Because $-NO_2$ moieties in **2** are hydrophilic,[13c] lower temperature promotes adsorbates to be hydrogen bonded to $-NO_2$ moieties rather than carboxylate groups.

Free-Energy Differences (ΔF_{host}) between the Two Guest-Free Forms. The free-energy difference (ΔF_{host}) between the two guest-free forms, wide pore and narrow pore, would be helpful for considering the ease of transformation. Two-step adsorption on jungle-gym-type porous coordination polymers proceeds via a wide → narrow → wide pore transition. Although the thermodynamics of the two concomitant processes, host−guest interactions and host structural transition, cannot be easily resolved experimentally, it is possible to calculate ΔF_{host} using a recently developed thermodynamic model.[27] This method relies on adsorption isotherms, which can be obtained experimentally. Figure 11a shows the applied results for IPA adsorption on **1** at 308 K. In two regions, 0.13−2.01 (blue) kPa for the narrow pore and 2.61−9.45 (red) kPa for the wide pore, each Langmuir curve is well fitted. Each of the produced osmotic thermodynamic potentials[27b] as a function of pressure for the narrow pore (blue) and wide pore (red) intersect at 2.13 kPa (= $P_{th,ad}$), another intersection being obtained at 0.32 kPa, indicating that shrinkage of framework **1** is completed at 0.32 kPa. The estimated ΔF_{host} value for **1** is 10−13 kJ mol^{-1}, which is smaller than the 16−19 kJ mol^{-1} for postsynthetic modified $[Zn_2(bdc\text{-}NH_2)_2(dabco)]_n$ (DMOF-1-AM3).[15] On the assumption that adsorption enthalpy, ΔH_{ad} (IPA), can simply be ascribed to the sum of ΔF_{host}, the heat of condensation of the guest molecules ($\Delta H_{g\text{-}g}$), and heat of interaction

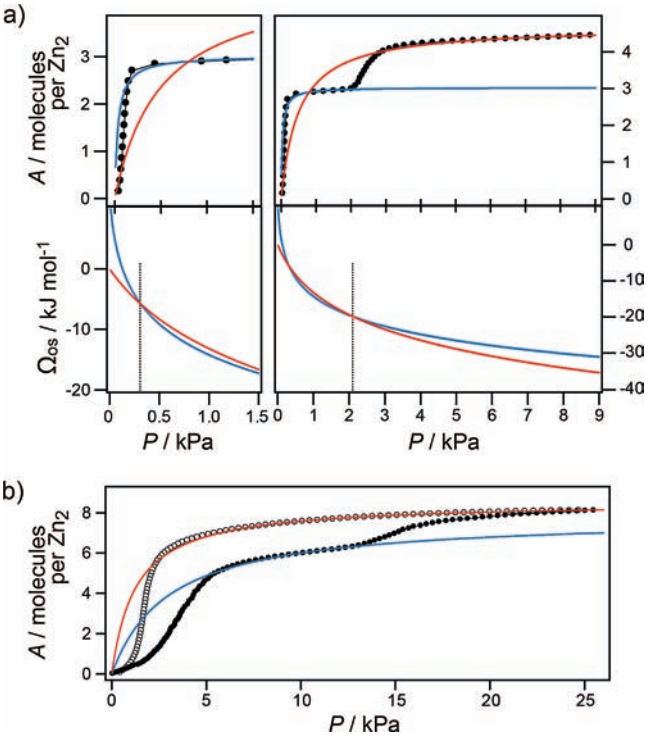

Figure 11. Experimental adsorption isotherms of (a) *i*-PrOH on **1** at 308 K and (b) MeOH on **2** at 308 K with Langmuir fittins. Langmuir fittings (upper) of *i*-PrOH adsorption isotmerm on **1** were carried out in 0.13−2.01 (blue) kPa and 2.61−9.45 (red) kPa regions. Osmotic thermodynamic potentials (below) as a function of pressure, calculated from the Langmuir fittings, are corresponding to the narrow pore (blue) and large pore (red) form of **1**. In the case of MeOH adsorption on **2**, Langmuir fittings were carried out in 5.11−12.74 kPa region of adsorption isotherm for the narrow pore (blue) form and 2.01−24.69 kPa region of desorption isotherm for the large pore (red) form.

(24) d(ln P)/d(T^{-1}) = $\Delta H_{ad}/R$ for the adsorption process, where R and ΔH_{ad} denote the gas constant and the adsorption enthalpy of the guest, respectively.

(25) Lide, D. R. *CRC Handbook of Chemistry and Physics*, 76th ed.; CRC Press: Boca Raton, FL, 1995.

(26) The results for IPA adsorption on **1** are reported in reference 13a.

(27) (a) Jeffroy, M.; Fuchs, A. H.; Boutin, A. *Chem. Commun.* **2008**, 3275–3277. (b) Coudert, F.-X.; Jeffroy, M.; Fuchs, A. H.; Boutin, A.; Mellot-Draznieks, C. *J. Am. Chem. Soc.* **2008**, *130*, 14294–14302. (c) Coudert, F.-X.; Mellot-Draznieks, C.; Fuchs, A. H.; Boutin, A. *J. Am. Chem. Soc.* **2009**, *131*, 3442–3443. (d) Boutin, A.; Springuel-Huet, M.-A.; Nossov, A.; Gédéon, A.; Loiseau, T.; Volkringer, C.; Férey, G.; Coudert, F.-X.; Fuchs, A. H. *Angew. Chem., Int. Ed.* **2009**, *48*, 8314–8317. (e) Coudert, F.-X.; Mellot-Draznieks, C.; Fuchs, A. H.; Boutin, A. *J. Am. Chem. Soc.* **2009**, *131*, 11329–11331.

between the guest molecules and the host ($\Delta H_{h\text{-}g}$), it is possible to estimate $\Delta H_{g\text{-}g}$ (IPA) + $\Delta H_{h\text{-}g}$ (IPA) values on two-step IPA adsorption on **1**: $\Delta H_{g\text{-}g,1}$ (IPA) + $\Delta H_{h\text{-}g,1}$ (IPA) = $-59.6 \sim -56.6$ kJ mol^{-1} and $\Delta H_{g\text{-}g,2}$ (IPA) + $\Delta H_{h\text{-}g,2}$ (IPA) = $-94.6 \sim -91.6$ kJ mol^{-1}.

In the case of MeOH adsorption/desorption on **2** at 308 K (Figure 11b), we succeeded in Langmuir fitting to the 5.11−12.74 kPa region of the adsorption isotherm for the narrow pore form (blue) and to the 2.01−24.69 kPa region of the desorption isotherm for the wide pore form (red). Interestingly, the estimated ΔF_{host} value for **2** is 1−3 kJ mol^{-1}, which is smaller than that of **1**. A smaller ΔF_{host} value, which shows the relative stability of the two phases, indicates that it is easier for **2** to go back and forth between the counterparts, wide and narrow pores. Because of this smaller energy difference between the two phases, the appearance of two-step MeOH adsorption on **2** strictly depends on the temperature.

Conclusion

This work was devoted to further understanding the two-step adsorption/desorption isotherms on jungle-gym-type porous coordination polymers. We have succeeded in synthesizing and characterizing novel ligand-substituted jungle-gym-type porous coordination polymers, $[Zn_2(bdc\text{-}NO_2)_2(dabco)]_n$ (**2**), $[Zn_2(bdc\text{-}Br)_2(dabco)]_n$ (**3**), and $[Zn_2(bdc\text{-}Cl_2)_2(dabco)]_n$ (**4**). Using various adsorbates, MeOH, EtOH, IPA, and Me_2CO, adsorption/desorption measurements were carried out on ligand-substituted jungle-gym-type porous coordination polymers **2**−**4** as well as $[Zn_2(bdc)_2(dabco)]_n$ (**1**), showing that two-step profiles were obtained in alcohol on **1** and MeOH on **2**. These results indicate that two-step adsorption is produced by the hydrogen bonds between the adsorbates and the carboxylate groups of the frameworks at the corners of the pores, leading to a wide to narrow pore transformation. Interestingly, the two-step profile found in MeOH adsorption on **2** depends on the temperature. As it would initially seem that the structural flexibility of these materials is related to the hydrogen-bonding nature of the probe gas molecule and frameworks, such results could pave the way for in-depth understanding of stepwise adsorption behaviors.

Acknowledgment. This work was supported by JGC-S Scholarship Foundation, the Kao Foundation for Arts and Sciences, and Mukai Science and Technology Foundation.

Supporting Information Available: Adsorption/desorption isotherms on **1**, TG, BET, and Langmuir plots of N_2 adsorption, XRPD, temperature dependences of *i*-PrOH and Me_2CO adsorption isotherms on **1**, DSC, and X-ray crystallographic files (CIF) for **3** and **4**. This material is available free of charge via the Internet at http://pubs.acs.org.